Earth, Planets and Space

FRONTIER LETTER

Open Access

Paleomagnetic studies on single crystals separated from the middle Cretaceous Iritono granite

Chie Kato[1,2*], Masahiko Sato[3], Yuhji Yamamoto[4], Hideo Tsunakawa[2] and Joseph L. Kirschvink[5,6]

Abstract

Investigations of superchrons are the key to understanding long-term changes of the geodynamo and the mantle's controlling role. Granitic rocks could be good recorders of deep-time geomagnetic field behavior, but paleomagnetic measurements on whole-rock granitic samples are often disturbed by alterations like weathering, and the presence of multi-domain magnetite. To avoid such difficulties and test the usefulness of single silicate crystal paleomagnetism, here we report rock-magnetic and paleomagnetic properties of single crystals and compare those to the host granitic rock. We studied individual zircon, quartz and plagioclase crystals separated from the middle Cretaceous Iritono granite, for which past studies have provided tight constraints on the paleomagnetism and paleointensity. The occurrence of magnetite was very low in zircon and quartz. On the other hand, the plagioclase crystals contained substantial amounts of fine-grained single-domain to pseudo-single-domain magnetite. Microscopic features and distinctive magnetic behavior of plagioclase crystals indicate that the magnetite inclusions were generated by exsolution. We therefore performed paleointensity experiments by the Tsunakawa–Shaw method on 17 plagioclase crystals. Nine samples passed the standard selection criteria for reliable paleointensity determinations, and the mean value obtained was consistent with the previously reported whole-rock paleointensity value. The virtual dipole moment was estimated to be higher than $8.9 \pm 1.8 \times 10^{22}$ Am^2, suggesting that the time-averaged field strength during middle of the Cretaceous normal superchron was several times as large as compared to that of non-superchron periods. Single plagioclase crystals which have exsolved magnetite inclusions can be more suitable for identification of magnetic signals and interpretation of paleomagnetic records than the conventional whole-rock samples or other silicate grains.

Keywords: Paleointensity, Granite, Single crystals, Feldspar, Zircon

Introduction

Long superchrons of constant geomagnetic polarity are the most distinctive features at the ~10 Myr scale trend of the geomagnetic field and are very possibly related to the whole-mantle convection process such as the activity of mantle plumes (e.g. Larson and Olson 1991; Glatzmaier et al. 1999; Courtillot and Olson 2007; Zhang and Zhong 2011; Biggin et al. 2012). Numerical dynamo simulations indicate that non-reversing stable dynamos with strong dipole moments will occur under conditions of relatively low CMB heat flow, whereas a reversing dynamo with multipolar nature is expected under conditions with high CMB heat flow (e.g. Kutzner and Christensen 2002; Christensen and Aubert 2006; Olson and Christensen 2006). Additionally, high dipole fields could be also caused by enhanced heterogeneity of CMB heat flow (e.g. Takahashi et al. 2008; Olson et al. 2010).

Understanding the geomagnetic field intensity during superchrons is crucial for revealing the nature of the long-term change of the geodynamo and the controlling role of the mantle on it. While dynamo simulations predict stronger field during superchrons, paleointensity

*Correspondence: chiekato15@gmail.com
[1] Department of Environmental Changes, Faculty of Social and Cultural Studies, Kyushu University, Fukuoka, Japan
Full list of author information is available at the end of the article

during the Cretaceous normal superchron (CNS) at 83–120 Ma has not reached consensus among previous paleomagnetic studies. Several studies suggest stronger field during CNS than the average for ages with frequent reversals (e.g. Tarduno et al. 2006; Tauxe 2006), while others claimed the opposite (e.g. Tanaka and Kono 2002; Shcherbakova et al. 2012). It is also challenging to get a solid conclusion from the paleomagnetic databases such as PINT (Biggin et al. 2009) and MagIC (earthref.org/MagIC) because the data deposited in them are mostly from volcanic rocks which reflect short-term geomagnetic variations and hide the long-term trends of paleointensity. In order to establish a reliable paleointensity curve for long-term variation, a brand new dataset based on appropriate samples and measurement methods is required.

To focus on the long-term variations of the past geomagnetic field, plutonic rocks could provide good candidate samples since they are likely to record the time-averaged field accurately during their long cooling history. Granites in particular have been formed at various ages and have preserved over geological time. However, paleomagnetic studies using granitic rocks are usually difficult due to weathering of the rocks and non-ideality of coarse grain multi-domain (MD) magnetite. Also, granitic rocks often contain biotite and pyrrhotite, which decompose easily upon laboratory heating and form some magnetite as a byproduct. One of the most promising approaches to overcome these difficulties is to separate single silicate crystals from them that contain magnetic mineral inclusions, and use them for paleomagnetic measurements.

Single silicate crystals with magnetic inclusions have the potential to yield reliable paleointensity data because the inclusions are more protected from chemical alternations such as oxic weathering in nature, and from thermochemical oxidation upon laboratory heating, than are the host granitic rocks. Zircon crystals have been used for paleointensity studies owing to its permanence against chemical alternation and ability to obtain direct radiometric ages on them (Tarduno et al. 2014, 2015), although Weiss et al. (2015) raised a controversy. Detailed rock-magnetic properties of zircons collected from river sand in the Tanzawa pluton, Japan, showed its adequacy for paleointensity measurements (Sato et al. 2015). Fu et al. (2017) reported that the absolute value of zircon paleointensity was consistent with the bulk rock using the Bishop Tuff of Northeastern California. Paleointensity and rock-magnetic properties have also been intensively studied on single plagioclase crystals which can contain magnetically stable fine-grained magnetite inclusions (Tarduno et al. 2006). For basalts from the 1955 Kilauea eruption, the recovered paleointensity has been compared with the whole-rock and magnetic observatory data, with good agreement (Cottrell and Tarduno 1999). Plagioclase crystals separated from lavas from the Rajmahal Traps (113–116 Ma; Tarduno et al. 2001), Strand Fiord Formation (95 Ma; Tarduno et al. 2002), Ocean Drilling Program (ODP) Site 1205 on Nintoku Seamount of the Hawaiian-Emperor volcanic chain and ODP Site 801 in the Pigafetta Basin (55.59 and 160 Ma, respectively; Tarduno and Cottrell 2005), and the Kiaman Reversed Superchron type area (~ 262–318 Ma; Cottrell et al. 2008) have been used for studies on paleointensity variation related to the reversal frequency of the dipole field. Quartz phenocrysts are also a target studied for Archean rocks (Tarduno et al. 2007, 2010, 2014). All of the paleointensity measurements mentioned above were taken using variants of the Thellier–Thellier method (Thellier and Thellier 1959; Coe 1967; Yu et al. 2004).

Rock-magnetic properties of plagioclase separated from plutonic rocks such as granitoids (Usui et al. 2015) and gabbros (Feinberg et al. 2005; Muxworthy and Evans 2012) have also been reported. Some of them are characterized by needle-shaped tiny magnetite inclusions possibly formed by exsolution from the host plagioclase (Feinberg et al. 2005; Usui et al. 2015; Wenk et al. 2011). Several preceding studies reported paleointensity estimates using plutonic rocks in which the authors argued that the magnetic records were carried by exsolved magnetite (Selkin et al. 2008; Usui 2013). Plagioclase with exsolved magnetite is potentially an excellent recording medium of the ancient geomagnetic field, but should be treated carefully because (1) magnetic remanence anisotropy caused by needle-shaped magnetite can affect paleomagnetic results (Paterson 2013; Usui et al. 2015), (2) nonlinear thermoremanence acquisition (Selkin et al. 2007), and (3) unknown formation temperature of exsolved magnetite (Feinberg et al. 2005). Usui and Nakamura (2009) reported paleointensity using single plagioclase crystals separated from a granitic rock, although they did not claim they achieved exact, reliable estimates. Despite its potential for establishing the long-term trend of the geomagnetic field strength, paleointensity of single crystals separated from plutonic rocks have not been compared to that of the host whole rock to assess its reliability.

This study aims to assess how paleointensity measurements on single silicate crystals separated from granitic rocks are reliable compared to those on whole-rock samples. We conducted systematic rock-magnetic measurements on zircon, quartz and plagioclase grains separated from whole-rock samples collected from the Cretaceous Iritono granite, a paleomagnetically well-studied unit in northeast Japan. The results suggest that plagioclase is the most appropriate candidate mineral for paleointensity measurements among the studied minerals. We

therefore conducted paleointensity experiments on plagioclase and compared the results with previously published results from the host granitic rock. Paleointensity experiments were conducted by the Tsunakawa–Shaw method (Tsunakawa and Shaw 1994; Yamamoto et al. 2003; Mochizuki et al. 2004; Yamamoto and Tsunakawa 2005; Yamamoto et al. 2015) which might be more suitable for single grain samples with exsolved magnetite than the variants of the Thellier–Thellier method. Obtained paleointensity results were consistent with the whole-rock data; thus it is suggested that plagioclase crystals separated from granitic rock have a potential to constrain the long-term variation of paleointensity.

Experimental methods

Sample description

We studied zircon, quartz and plagioclase separated from the middle Cretaceous Iritono granite in the Abukuma massif, northeast Japan (Fig. 1). Cooling history of the Iritono granite is constrained by Wakabayashi et al. (2006) and Tsunakawa et al. (2009) using a thermal diffusion model of the granite body, and by two radiometric age determinations with different closure temperatures. The U–Pb zircon age is 115.7 ± 1.9 Ma (Tsunakawa et al. 2009) and the ^{40}Ar–^{39}Ar biotite age is 101.9 ± 0.2 Ma (Wakabayashi et al. 2006). The age of the Iritono granite corresponds to the middle part of the CNS, in which the polarity reversals had been stopped for a period as long as 20 Myr. The estimated cooling time for a lock-in of a paleomagnetic record is 4×10^4 to 1.4×10^7 years. Wakabayashi et al. (2006) and Tsunakawa et al. (2009) previously conducted rock-magnetic and paleomagnetic studies and paleointensity experiments on the whole-rock samples of the Iritono granite. The magnetic minerals in the Iritono granite were magnetite and pyrrhotite, and their fraction varied with sampling locations. Samples from site ITG09 showed the least contribution of pyrrhotite, and the primary magnetization was clearly distinguished from the secondary magnetization carried by low blocking temperature or low coercivity components in terms of natural remanent magnetization (NRM) direction. Tsunakawa et al. (2009) studied the paleointensity by both the Coe's version of Thellier method (Thellier and Thellier 1959; Coe 1967) and the Tsunakawa–Shaw method using the whole-rock sample of site ITG09. Although the obtained paleointensities exhibit a bimodal distribution according to the different methods used, they were indistinguishable at the 2σ level and thus were combined into one site-mean. The resultant site-mean paleointensity was 58.4 ± 7.3 μT before applying the cooling rate correction, and 39.0 ± 4.9 μT after correction. This corresponds to a virtual dipole moment (VDM) of $9.1 \pm 1.1 \times 10^{22}$ Am^2. The present study used the mineral samples separated from the core samples of site ITG09.

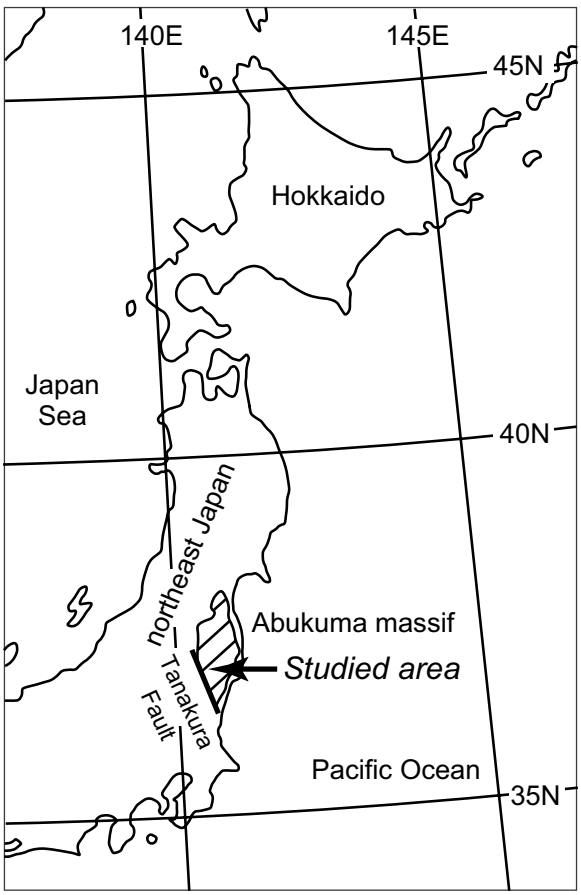

Fig. 1 Map of the Iritono granite in the Abukuma massif, northeast Japan (reproduced from Wakabayashi et al. 2006)

Sample preparation

A granite sample core 2.54 cm in diameter was crushed with a non-magnetic mortar and pestle, and sorted by 850 μm and 350 μm mesh screens. Heavy fractions of the sample smaller than 350 μm were concentrated by an aqueous panning technique. Zircons with no visible cracks or opaque particles on the surface were hand-picked under a binocular stereoscopic microscope. Quartz and plagioclase were hand-picked from samples larger than 350 μm and smaller than 850 μm. These selected crystals were leached by hydrochloric acid (HCl) to remove any tiny magnetic particles on the sample surface. HCl concentration and leaching duration was 12 N and 4 days for zircon and quartz, and 6 N and 8 h for plagioclase, respectively. Samples were then sandwiched individually between layers of magnetically clean Scotch Magic Transparent Tape in the method of Sato et al.

(2015) or were mounted individually on a glass holder (see below) for rock-magnetic measurements and paleointensity experiments.

Remanence measurements using SQUID magnetometer

A superconducting quantum interference device (SQUID) magnetometer (2G Enterprises Model 755-4.2 cm) was used for remanence measurements. We followed the method of single-crystal measurements by Sato et al. (2015). A sample holder made of acrylonitrile butadiene styrene (ABS) was used for measurements. Single-crystal samples sandwiched by tape or mounted on the glass holder were fixed on the edge of the ABS holder by double-stick tape. The magnetic moments of the ABS holder and double-stick tape were measured before and after sample measurement and subtracted from the sample moment. The detection limit of the method was 2×10^{-12} Am^2, so we employed 4×10^{-12} Am^2 as a threshold to distinguish significant remanence intensity from noise.

For stepwise thermal demagnetization (ThD) and paleointensity experiments, we made new thermally resistant holders for single-crystal measurement of the SQUID magnetometer based on the sample holder designed for SQUID microscope measurements (Fu et al. 2017). Images of the sample holder are shown in Fig. 2. Non-alkali high-temperature glass plates (Eagle XG, Corning, 1.1 mm thick) were cut into squares of 7 mm on a side. A 1-mm-diameter pit was drilled in the center of the glass plate, followed by intense cleaning in concentrated HCl. A single-crystal sample was put into the pit and fixed by stuffing SiO_2 powder with grain size of ~0.8 μm. This technique enabled us to conduct heating experiments on single crystals in a fixed sample coordinate. The blank magnetic moment of the glass holder after subtracting the moment of ABS holder and double-stick tape was well below the practical detection limit of the SQUID magnetometer.

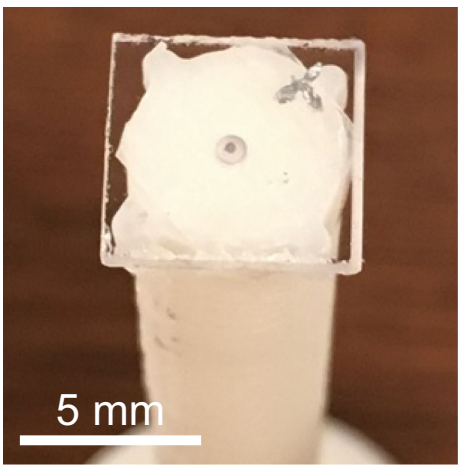

Fig. 2 Image of the glass holder fixed on the ABS holder. 7 mm each side. A plagioclase grain can be seen through the glass in the center

First, we measured NRM intensity of 349, 455, and 268 grains for zircon, quartz, and plagioclase, respectively. On the basis of the NRM intensities, we then selected samples for further rock-magnetic and paleomagnetic measurements.

Rock-magnetic measurements

For the selected samples that showed significant NRM intensity ($> 4 \times 10^{-12}$ Am^2 per grain), we conducted low-temperature remanence measurements using a magnetic property measurement system (Quantum Design model MPMS-XL5). Isothermal remanent magnetization (IRM) was first imparted at 2.5 T and 10 K after zero-field cooling from 300 K. The remanence was then measured during warming in zero-field (ZFC remanence). Subsequently, samples were cooled to 10 K in a 2.5 T field and then remanence was further measured during warming in zero-field (FC remanence).

Hysteresis loop measurements were taken for plagioclase grains and a quartz grain which contained magnetite using an alternating gradient magnetometer (LakeShore model MicroMag 2900). Samples sandwiched by tape were mounted on a transducer probe with a silica sample stage (Lake Shore model P1 probe). The blank saturation magnetization of the probe was 6×10^{-10} Am^2. Maximum field during hysteresis loop measurement was 0.5 T, and the field increment was 4 mT. Diamagnetic/paramagnetic corrections were applied to the obtained hysteresis loop by subtracting the average slopes at applied field of $|\boldsymbol{B}| > 300$ mT. Results are exhibited in the Day plot (Day et al. 1977).

Stepwise ThD of NRM was performed on selected zircon and quartz samples using a TDS-1 thermal demagnetizer (Natsuhara Giken). For plagioclase samples, stepwise ThD of laboratory-imparted thermoremanent magnetization (TRM) was performed after paleointensity experiments. TRM was given by cooling from 610 °C in a 50 μT field in air.

To investigate the NRM to IRM (NRM/IRM) distribution of plagioclase, a room-temperature IRM was imparted to 75 plagioclase samples at 2 T by an MMPM10 pulse magnetizer (Magnetic Measurements), and the IRM intensity was measured using the SQUID magnetometer.

Paleointensity experiments

We performed paleointensity experiments with the Tsunakawa–Shaw method on 17 plagioclase grains. We followed the procedures described in Yamamoto and

Tsunakawa (2005). In this method, stepwise alternating field demagnetization (AFD) of NRM and TRM is performed. Assuming the similarity of TRM and anhysteretic remanent magnetization (ARM), alternation caused by laboratory heating is monitored by comparing the coercivity spectra of ARMs before heating (ARM_{before}) and after (ARM_{after}). TRM is corrected by:

$$TRM^* = TRM \times ARM_{before}/ARM_{after} \quad (1)$$

where TRM* is the corrected TRM. Paleointensity is determined using the slope in the TRM*–NRM diagram. The samples are heated twice. Assuming that thermal alternation in the first and second heating is similar, the validity of the ARM correction for alternation was checked by the second heating by comparing the measured intensity to the laboratory field. Samples are subjected to low-temperature demagnetization (LTD) before each stepwise AFD series to selectively demagnetize the unstable coarse grain magnetite. LTD treatment was conducted by cooling a sample in a dewar bottle inside a triple magnetically shielded case filled with liquid nitrogen for 5 min. TRM was given by cooling from 610 °C in a 50 μT field in a vacuum (< 10 Pa). The heating time at the top temperature of 610 °C was 10 (20) minutes for first (second) heating, with a subsequent cooling to room temperature with a rate of approximately 10 °C per minute. AFD treatment and ARM impartment was carried out using an alternating field demagnetizer (Natsuhara Giken model DEM-95C). AFD was conducted during sample tumbling. ARM was imparted at DC field of 50 μT, with a peak AC field of 180 mT. Here we define ARM0, ARM1 and ARM2 as the ARM imparted before heating, after first heating and after second heating, respectively. Also, TRM1 and TRM2 are given by the first and second heating, respectively. The corrected TRMs, TRM1* and TRM2* are given by TRM1 × ARM0/ARM1 and TRM2 × ARM1/ARM2, respectively. Paleointensity value is calculated by the slope of the NRM–TRM1* plot. The field intensity calculated from the slope of the TRM1–TRM2* plot is compared to the laboratory field intensity. We attempted to deal with the anisotropy effect on paleointensity by two experimental protocols. For four samples (sample IDs of 9004, 9009, 9013 and 9016), all ARMs and TRMs were given along the likely direction of the characteristic remanent magnetization (ChRM), estimated from the orthogonal plot of AFD of the NRM, so that the anisotropy bias was canceled. For the others we followed the standard protocol of the Tsunakawa–Shaw method in which ARM0 is approximately parallel to ChRM and ARM1 (ARM2) is parallel to TRM1 (TRM2). This protocol employs a built-in anisotropy correction using ARMs (Yamamoto et al. 2015); the anisotropy bias caused by angular difference between NRM (TRM1) and TRM1 (TRM2) is corrected by ratios of ARM0/ARM1 (ARM1/ARM2). In the present study, ARM1, ARM2, TRM1 and TRM2 were imparted along the Y axis, which is independent of the direction of ChRM. In this study, AFD steps for ARMs without LTD treatment (ARM00, ARM10, and ARM20) were omitted.

Remanence anisotropy measurements

To assess anisotropy effect, we measured the ARM anisotropy of 19 plagioclase samples including 13 samples which were subjected to the paleointensity experiments. ARM was imparted along three orthogonal axes (ARM_x, ARM_y, and ARM_z) to obtain the remanence anisotropy tensor. Measurements were taken after LTD treatments. TRM anisotropy tensor was also measured after paleointensity experiments for some samples and the consistency with the ARM anisotropy tensor was checked. The ARM and TRM measurements were also taken after AFD with a peak AC field of 50 mT. ARM anisotropy of whole-rock samples was checked based on measurement results obtained using a spinner magnetometer (Natsuhara Giken model SMD88).

Results

Rock-magnetic properties of zircon

Sixteen out of 349 zircon samples had NRM intensities larger than the threshold (Fig. 3a). Low-temperature magnetometry and stepwise ThD measurements of NRM were taken on selected samples that had significant NRM intensity. Representative results are summarized in Fig. 4. Stepwise ThD treatment for NRM was performed on four samples. Two samples showed a characteristic magnetization component and pyrrhotite-like blocking temperature (Fig. 4a), but the other two did not show any stable remanence component (Fig. 4b). Low-temperature experiments were performed on additional five samples. One sample showed a phase transition of pyrrhotite at ~30 K (Fig. 4c), while the other four samples did not show any obvious transition (Fig. 4d). We concluded that the dominant magnetic inclusion in zircon is pyrrhotite and/or magnetically very soft materials. Since the whole-rock study determined that a low blocking temperature (< 400 °C) component is probably carried by pyrrhotite and hence was most likely remagnetized by a reheating event (Wakabayashi et al. 2006), we did not use zircon for paleointensity experiments.

Rock-magnetic properties of quartz

Similar to the zircon samples, very few samples of quartz (7 out of 455) had NRM intensities larger than the threshold (Fig. 3b). We took stepwise ThD measurements of NRM on two quartz grains. In both samples, magnetization decreased generally toward the origin in

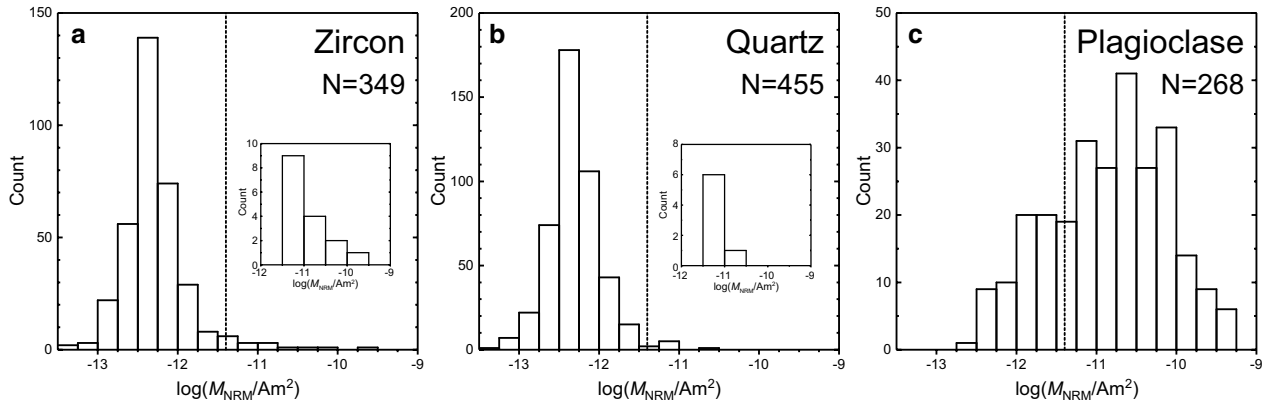

Fig. 3 Histogram of NRM intensity of **a** zircon, **b** quartz and **c** plagioclase. Dotted lines indicate the threshold for significant remanence. Inset figures in **a** and **b** show the histogram of NRM intensity above the threshold (4×10^{-12} Am^2)

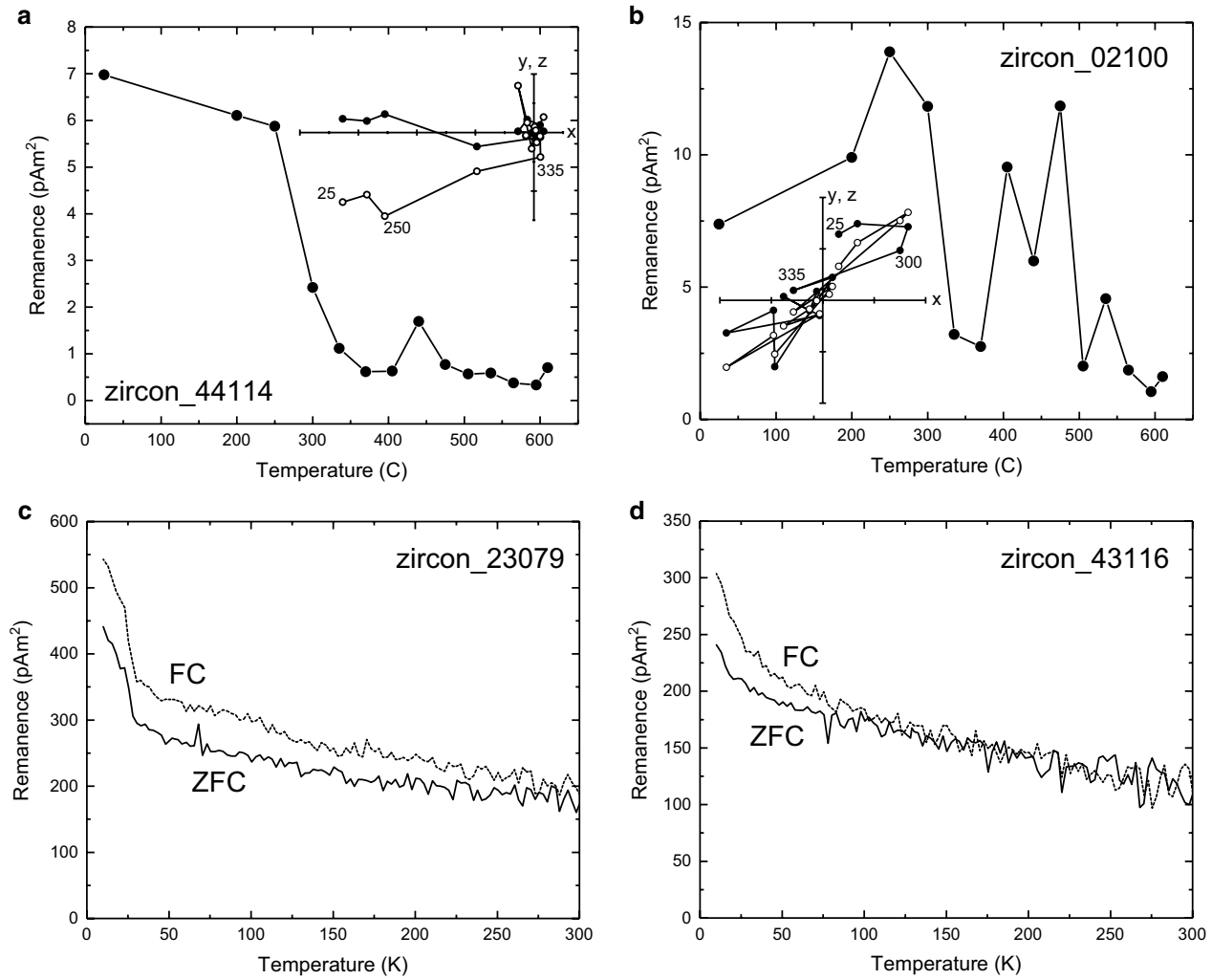

Fig. 4 Results of experiments on selected zircon. **a**, **b** Stepwise ThD of NRM. In the orthogonal plot, open and closed circles indicate *X*–*Y* and *X*–*Z* planes, respectively. **c**, **d** Low-temperature remanence measurements. Solid lines for ZFC measurements and dotted lines for FC measurements

the orthogonal plot. One sample shows a high blocking temperature suggesting magnetite inclusion (Fig. 5a) and the other sample exhibits a lower, pyrrhotite-like blocking temperature (Fig. 5b). We further took low-temperature magnetometry measurements and hysteresis loop measurements on the former sample. The Verwey transition of magnetite was recognized near 120 K (Fig. 5c) that indicate titanium-poor magnetite (Özdemir et al. 1993; Moskowitz et al. 1998). High coercivity ($B_c > 10$ mT) exhibited in the slope-corrected hysteresis loop suggests the existence of fine-grained magnetite. We concluded that quartz is a potentially ideal sample for paleomagnetic study. However, we decided not to use quartz for paleointensity experiments because it was difficult to find enough magnetite bearing samples to study.

Rock-magnetic properties of plagioclase

A histogram of NRM intensity for the plagioclase crystals is shown in Fig. 3c. In contrast to the zircon and quartz samples, very high population of the plagioclase samples (224 out of 268; 84%) exhibited the significant NRM intensities. Figure 6a shows a diagram between NRM intensities and IRM intensities for the 75 plagioclase grains. NRM/IRM distributes in a narrow range, namely around 0.1 (Fig. 6b), indicating the similar magnetic carrier and NRM origin among the plagioclase grains. The NRM/IRM ratio around 0.1 is higher than the TRM(50 μT)/IRM ratio for synthetic samples which resemble rocks (Yu 2010), and consistent with, but somewhat lower than the previous reports

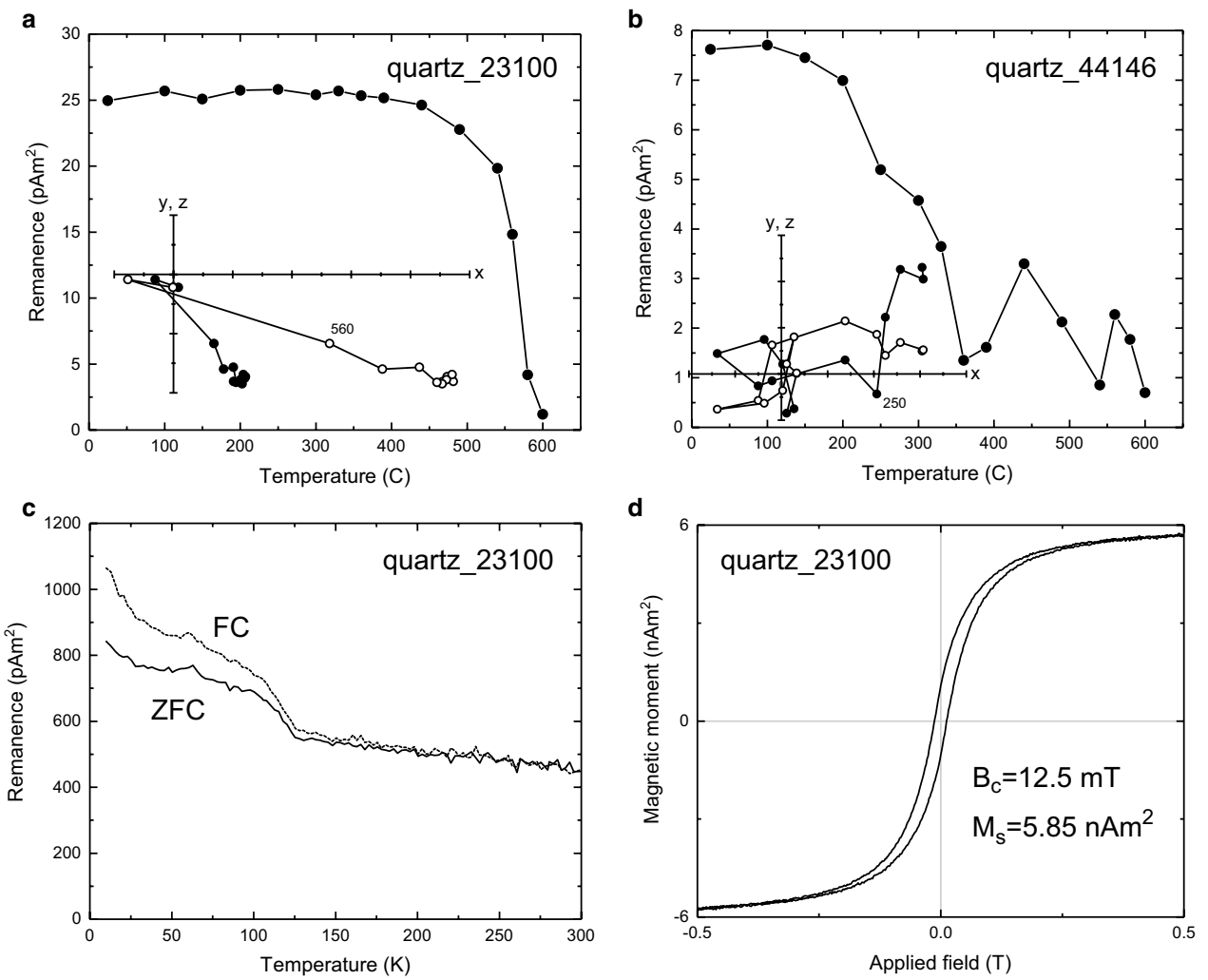

Fig. 5 Results of experiments on selected quartz. **a**, **b** Stepwise ThD of NRM. In the orthogonal plot, open and closed circles indicate *X*–*Y* and *X*–*Z* planes, respectively. **c** Low-temperature remanence measurements. Solid lines for ZFC measurements and dotted lines for FC measurements. **d** Hysteresis loop after slope correction. The slope correction coefficient was + 74.8 nAm^2/T

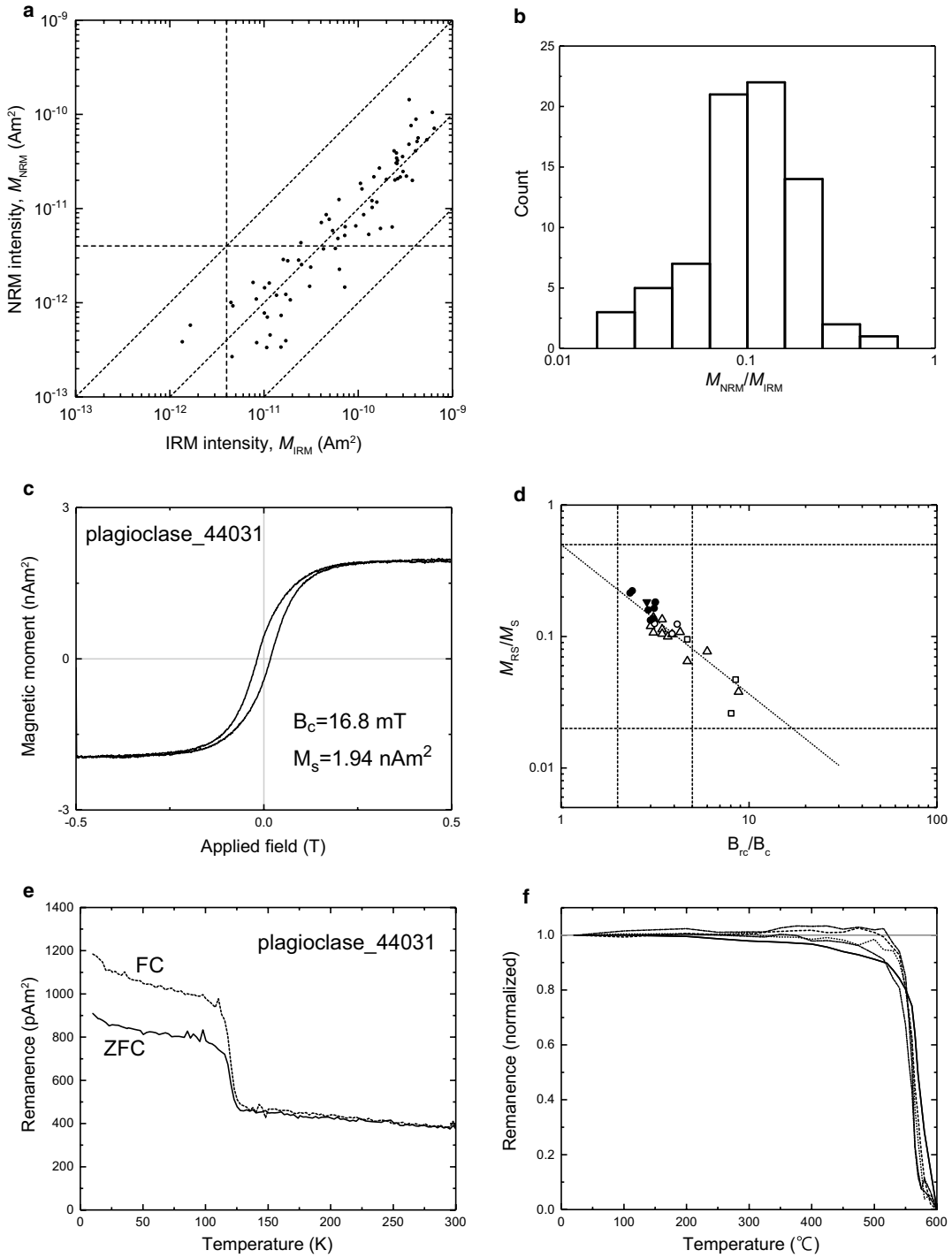

Fig. 6 Results of experiments on plagioclase. **a** NRM intensity plotted as a function of IRM intensity. Horizontal and vertical dashed lines indicate the threshold for significant remanence. **b** Histogram of NRM intensity divided by IRM intensity. **c** Representative hysteresis loop after slope correction. The slope correction coefficient was +61.4 nAm^2/T. **d** Day plot of quartz and plagioclase grains shown with previous reports by Wakabayashi et al. (2006). Closed symbols represent results of this study. Reversed triangle indicates quartz, and circle indicates plagioclase. Opened symbols represent results of Wakabayashi et al. (2006). Triangle, circle and square indicate non-separated chips, feldspar fraction and biotite fraction, respectively. Dotted lines show the SD-MD magnetite mixture trend after Channell and McCabe (1994) and Parry (1982). **e** Low-temperature remanence measurements. Solid lines for ZFC measurements and dotted lines for FC measurements. **f** Stepwise ThD of TRM given at 50 μT compared to that of TRM1 of the whole-rock sample ITG09b-34-1 (Wakabayashi et al. 2006). Dashed lines for plagioclase grains and solid line for whole rock. Solid gray line indicates TRM value before ThD

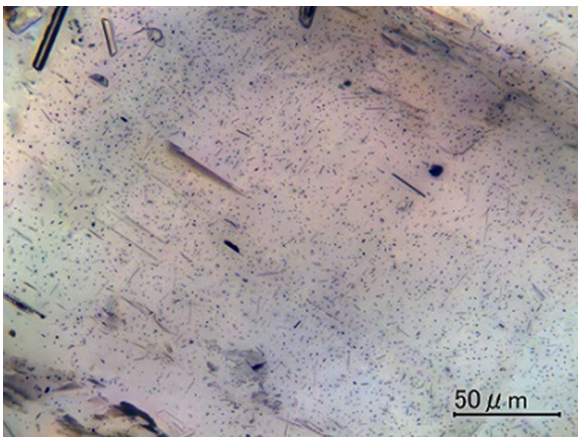

Fig. 7 Microscopic image of a polished single plagioclase crystal. Stacking of snaps of different focal depths

on plagioclase crystals (Usui et al. 2015) or rocks containing exsolved magnetite (Selkin et al. 2007).

We performed magnetic hysteresis and low-temperature magnetometry measurements on four selected grains with different NRM/IRM ratios. All of the four samples exhibited similar features in both hysteresis and low-temperature magnetization. Results on the hysteresis measurements fall in the PSD region of a Day plot (Fig. 6d) and are concentrated in a narrower region of the diagram compared to the whole rock. This indicates that the magnetite in plagioclase crystals has narrower range of grain size than that in the whole rock. The Verwey transition of magnetite was clearly observed at approximately 120 K (Fig. 6e), indicating a very low titanium content of magnetite (Özdemir et al. 1993; Moskowitz et al. 1998). Larger remanence in the FC curve relative to the ZFC curve (Fig. 6e) also suggests a dominance of fine-grained magnetite (Moskowitz et al. 1993; Carter-Stiglitz et al. 2001, 2002; Kosterov 2003).

After paleointensity measurements, we took hysteresis measurements on four samples and low-temperature measurements on one sample. The results were similar to those shown in Fig. 6c, e, which implies that the double heating during paleointensity measurements did not severely affect the magnetic characteristics of plagioclase grains. A distribution of the blocking temperature was investigated on four samples after paleointensity experiments. Results show a very narrow blocking temperature distribution around 530–580 °C (Fig. 6f).

Figure 7 is a microscopic image of a polished plagioclase sample (sample no. 68 in Table 2). The tiny opaque minerals with rounded to needle-like shapes are uniformly distributed in the host plagioclase and showed no association with cracks. These opaque minerals are probably magnetite, and the texture implies that the magnetites were not generated by secondary alternation but rather have a primary origin such as incorporation during plagioclase crystallization or exsolution at subsolidus conditions. Furthermore, the needle-like shape of magnetite and their preferred alignment relative to the feldspar suggests an origin via exsolution because magnetite tends to form equant octahedral crystals when crystallizing from a magma. The needle-like grains could be categorized to SD state due to particle length (few micron in most but up to > 10 um) and width length ratio of < 0.1 (Dunlop and Özdemir 1997). The round-shaped grains are possibly in the PSD state.

To summarize, rock-magnetic measurements of plagioclase samples indicate that the plagioclase crystals contain nearly-pure needle-like-shaped SD and PSD magnetite with width less than a few micron and various aspect ratio and are suitable for paleointensity measurements.

Paleointensity experiments of plagioclase

We conducted Tsunakawa–Shaw paleointensity experiments on 17 plagioclase grains. In consideration of the sensitivity of the instrument, samples with NRM intensities larger than 5×10^{-11} Am^2 were chosen for the experiments. Taking weak remanences of single-crystal samples into account, we employed a slightly different selection criteria from the study by Yamamoto and Tsunakawa (2005) which worked on strong remanences of volcanic whole rocks. The criteria we adopted are:

1. A primary component found in an orthogonal plot of NRM demagnetization
2. $f > 0.3$ in a NRM–TRM1* plot
3. $R > 0.90$ in a NRM–TRM1* plot
4. Slope of a TRM1–TRM2* plot within 1 ± 0.1
5. $R > 0.95$ in a TRM1–TRM2* plot

where f is the NRM fraction of the primary component and R is the correlation coefficients. Primary components were identified on an orthogonal plot of NRM, and it associated with MAD values < 16°. By the LTD treatment, 5–15% of the NRM was demagnetized. The demagnetized components by LTD are attributed to the remanence carried by PSD magnetite (Heider et al. 1992). By the above criteria, 9 out of 17 results were selected: two results were rejected by the criteria of 1 and/or 3; six results were rejected due to the criterion of 4. Typical examples of successful and rejected results are, respectively, presented in Figs. 8, 9 and 10. Results of all 17 samples are summarized in Table 1. Paleointensities obtained from the nine results range between 43.1 and 77.9 μT, yielding an average of 57.4 μT

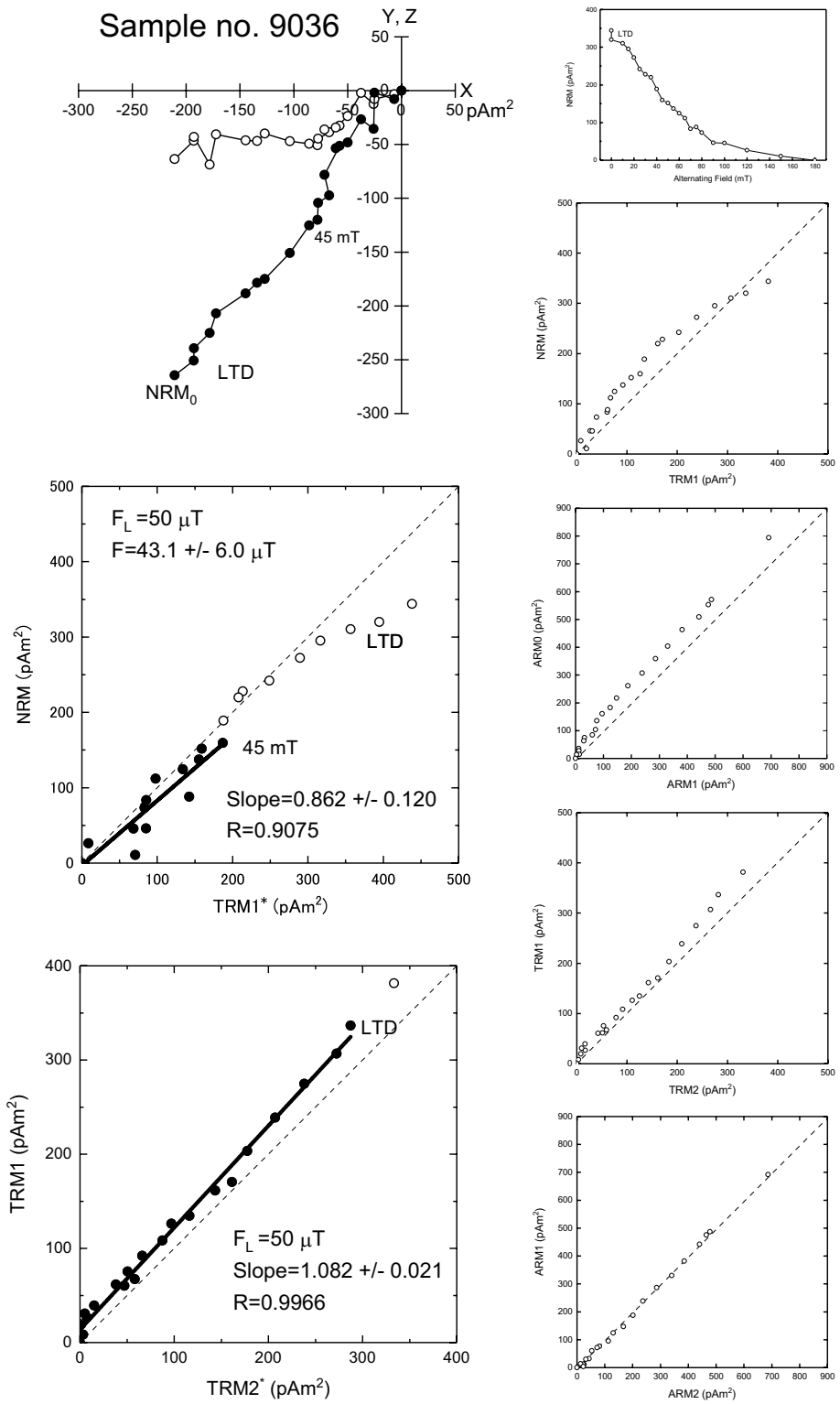

Fig. 8 A representative result of successful paleointensity measurements by the Tsunakawa–Shaw method on single plagioclase grain. The dotted line indicates where the horizontal and vertical axes are equal. In the orthogonal plot, open and closed circles indicate *X–Y* and *X–Z* planes, respectively

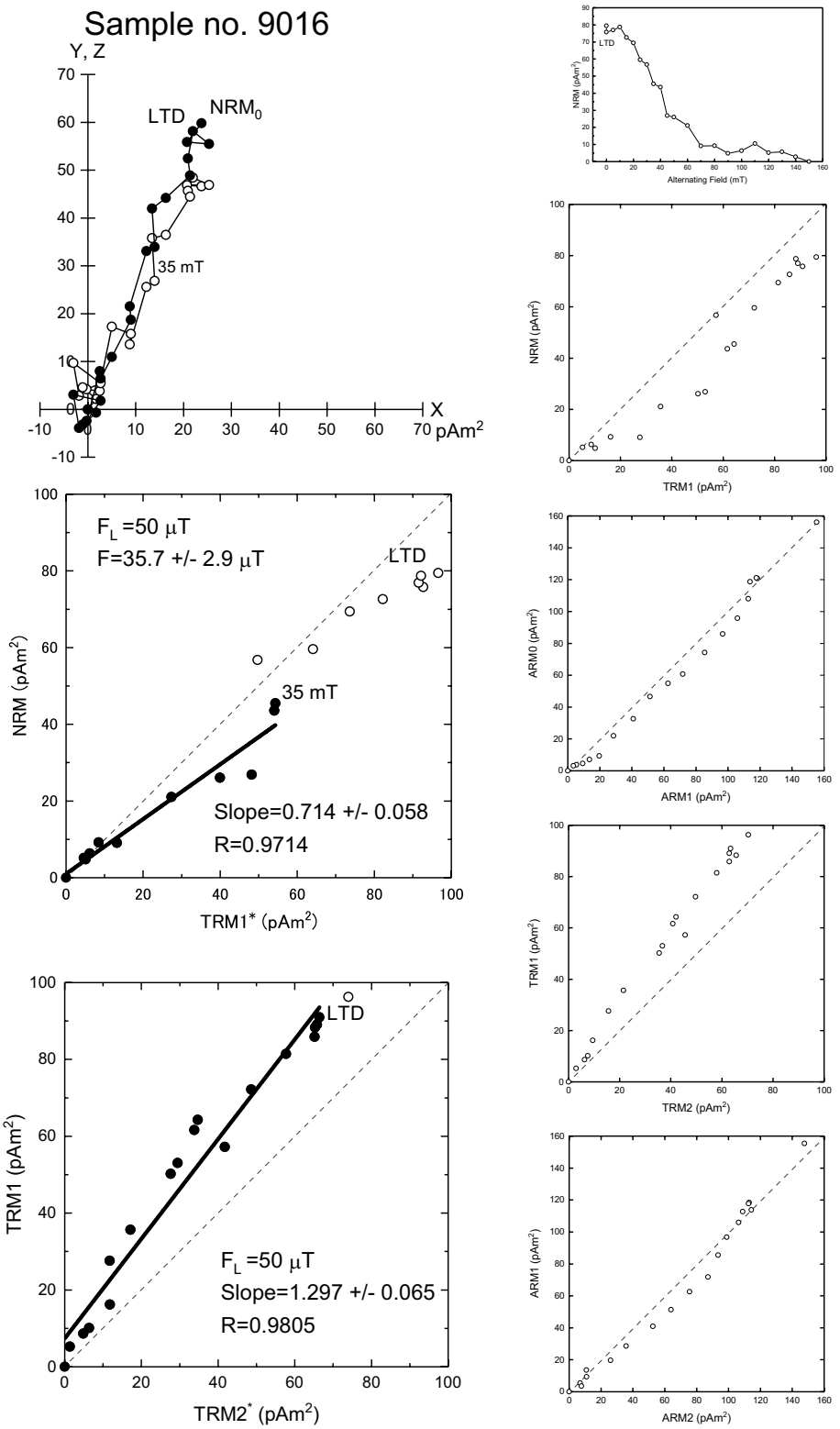

Fig. 9 Example of failed paleointensity measurements by the Tsunakawa–Shaw method on single plagioclase grain. In the orthogonal plot, open and closed circles indicate *X–Y* and *X–Z* planes, respectively. TRM1/TRM2* slope severely exceeds 1

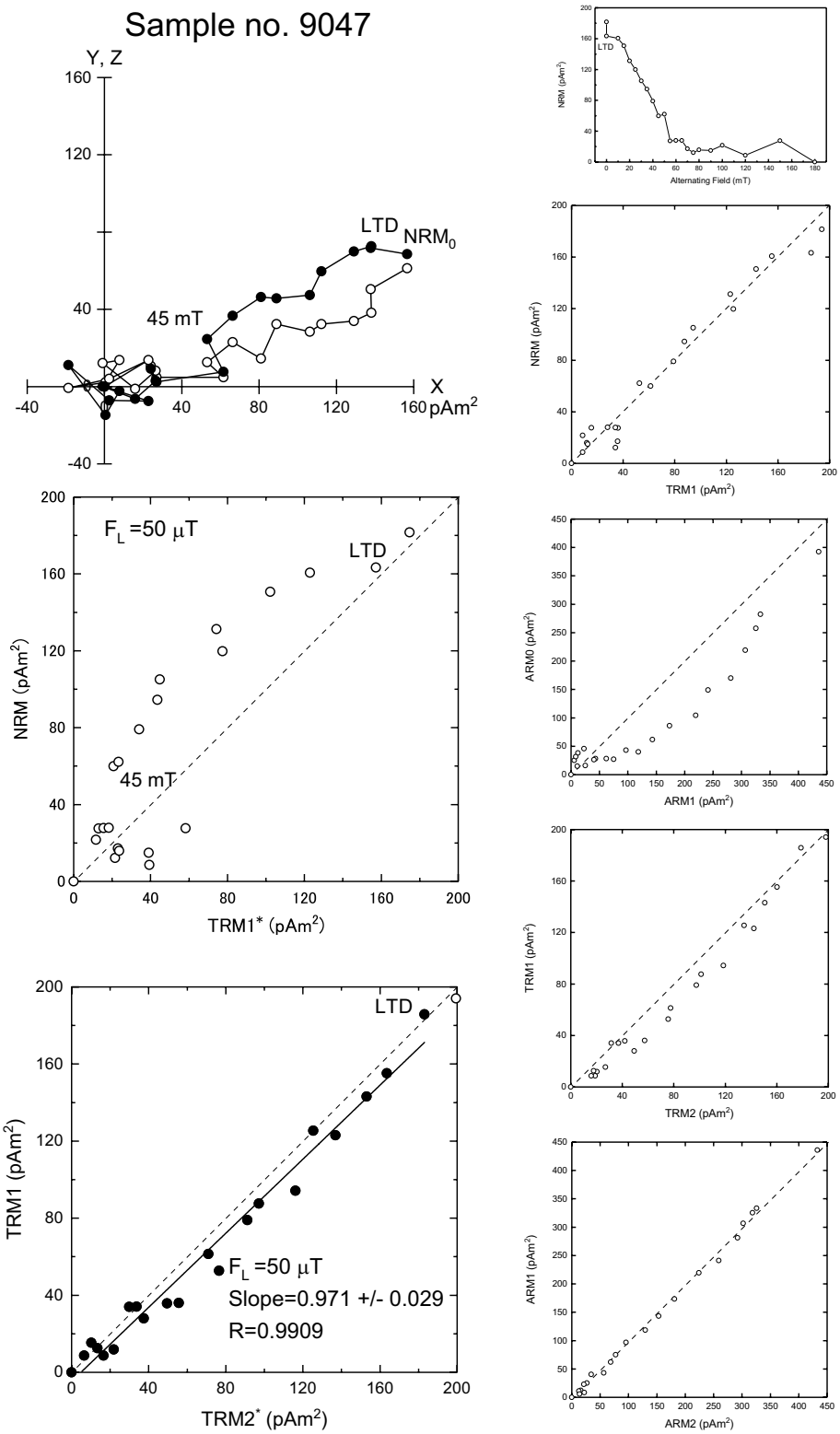

Fig. 10 Example of failed paleointensity measurements by the Tsunakawa–Shaw method on single plagioclase grain. In the orthogonal plot, open and closed circles indicate *X–Y* and *X–Z* planes, respectively. No linear portion in the NRM/TRM1* plot

Table 1 Results on Paleointensity measurements of plagioclase samples

Sample ID	NRM_0 (pAm^2)	H_L (mT)	*f*	MAD (°)	ARM0 (pAm^2)	NRM–TRM1*		TRM1–TRM2*		
						Slope	*R*	Slope	*R*	*F* (μT)
Successful samples										
9004	134.6	0	1.000	9.2	248.7	0.945 ± 0.064	0.9647	1.054 ± 0.050	0.9827	47.2 ± 3.2
9009	93.0	40	0.700	9.8	147.2	1.142 ± 0.100	0.9706	1.094 ± 0.021	0.9972	57.1 ± 5.0
9020	484.0	45	0.486	9.2	616.5	1.253 ± 0.083	0.9658	1.048 ± 0.026	0.9944	62.6 ± 4.2
9036	344.0	45	0.499	10.2	794.1	0.862 ± 0.120	0.9075	1.082 ± 0.021	0.9966	43.1 ± 6.0
9099	193.1	0	1.000	11.0	319.0	1.558 ± 0.126	0.9456	1.051 ± 0.056	0.9744	77.9 ± 6.3
9054	264.8	35	0.570	15.9	355.1	1.457 ± 0.187	0.9075	1.078 ± 0.061	0.9710	72.8 ± 9.4
9070	126.7	15	0.942	12.9	336.0	0.974 ± 0.096	0.9259	0.968 ± 0.032	0.9900	48.7 ± 4.8
34,019	104.0	20	0.868	11.0	265.5	1.129 ± 0.106	0.9394	0.960 ± 0.031	0.9908	56.4 ± 5.3
44,092	64.7	10	0.992	10.6	117.1	1.007 ± 0.096	0.9301	1.008 ± 0.041	0.9851	50.3 ± 4.8
									Mean	57.4 ± 11.8
Failed samples										
9013	90.8	35	0.677	7.9	106.9	1.424 ± 0.095	0.9785	0.887 ± 0.051	0.9728	71.2 ± 4.7
9016	79.5	35	0.600	11.1	156.0	0.714 ± 0.058	0.9714	1.297 ± 0.065	0.9805	35.7 ± 2.9
9035	269.6	No primary magnetization			552.5	–	–	0.961 ± 0.035	0.9872	
9047	181.6	Low linearity in NRM/TRM1* plot			392.7		–	0.971 ± 0.029	0.9909	
9061	174.4	20	0.860	8.9	335.7	0.935 ± 0.086	0.9420	1.232 ± 0.070	0.9705	46.7 ± 4.3
9113	495.7	25	0.855	8.9	624.4	1.611 ± 0.111	0.9662	1.173 ± 0.065	0.9722	80.6 ± 5.6
44,106	88.5	20	0.923	5.9	120.5	1.216 ± 0.104	0.9465	0.849 ± 0.078	0.9276	60.8 ± 5.2
44,108	76.2	0	1.000	5.3	132.4	1.310 ± 0.062	0.9847	0.627 ± 0.119	0.7706	65.5 ± 3.1

NRM0 NRM intensity before LTD, H_L the lowest AFD step used in paleointensity estimate, *f* NRM fraction of the primary magnetization used in paleointensity estimate, *ARM0* intensity of ARM0 before LTD, *R* correlation coefficient, *F* estimated paleointensity

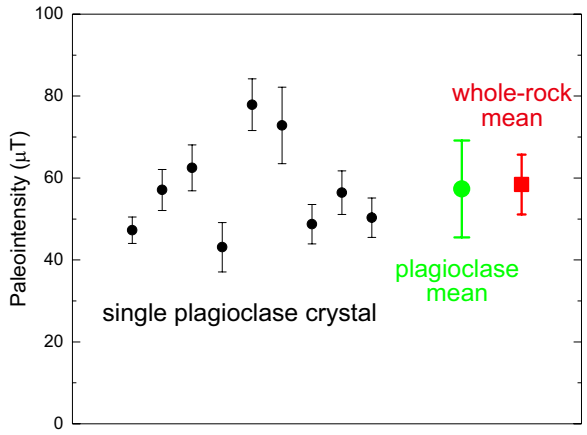

Fig. 11 Summary of paleointensity and error (1σ) of plagioclase compared with the whole rock. Black circles indicate results of each plagioclase grain. Green circle denotes the mean of nine plagioclase grains. Red square marks the mean of whole-rock measurements (Tsunakawa et al. 2009)

and a standard deviation of 11.8 μT. Figure 11 shows an individual plagioclase paleointensity as well as their average together with the average paleointensity reported from the whole rocks. The plagioclase average is in good agreement with the average paleointensity reported from the whole rocks, though the dispersion of plagioclase paleointensity is slightly larger than that of the whole rocks.

Two protocols were employed for handling the anisotropy bias on paleointensity ("Paleointensity experiments" section). In both protocols, it was technically difficult to impart ARM0 accurately parallel to ChRM. Therefore, the anisotropy bias on each sample would not be corrected completely. The angular differences between ChRM and ARM0 were 24° at most. The possible canceling of anisotropy bias by averaging a number of samples is discussed in "Anisotropy effect on paleointensity" section. The protocol in which ARM1, ARM2, TRM1 and TRM2 were given

Table 2 Anisotropy parameters of plagioclase samples

Sample name	Mean ARM (10^{-10} Am^2)	Eigen values of remanence tensor			P_j	T_j
		w_1	w_2	w_3		
9020	3.22	1.70	0.81	0.49	3.51	−0.20
9036	4.49	1.56	1.01	0.43	3.72	0.32
9099	1.77	1.50	0.92	0.58	2.60	−0.03
9054	2.14	1.42	0.93	0.65	2.19	−0.08
9070	2.14	1.36	0.90	0.74	1.87	-0.38
34,019	1.64	1.60	1.07	0.33	5.18	0.49
44,092	0.95	1.43	1.09	0.48	3.10	0.50
9035	3.06	1.40	0.86	0.74	1.96	−0.51
9047	2.54	1.23	1.04	0.73	1.70	0.37
9061	1.58	1.64	0.88	0.48	3.41	0.00
9113	3.08	1.57	0.83	0.60	2.68	−0.31
44,106	0.85	1.58	0.85	0.57	2.78	−0.23
44,108	0.71	1.48	0.80	0.71	2.19	−0.67
11	1.16	1.65	0.86	0.49	3.35	−0.07
12	2.22	1.95	0.68	0.37	5.41	−0.26
16	1.81	1.56	0.99	0.44	3.58	0.28
36	2.14	1.64	0.92	0.44	3.76	0.12
55	1.91	1.48	1.20	0.32	5.17	0.72
68	1.35	1.79	0.64	0.57	3.52	−0.80
Median		1.56	0.90	0.49		

Mean ARM average of the eigenvalues of ARM anisotropy tensor, w_1, w_2 and w_3 maximum, medium and minimum eigenvalue of ARM anisotropy tensor normalized by the mean ARM

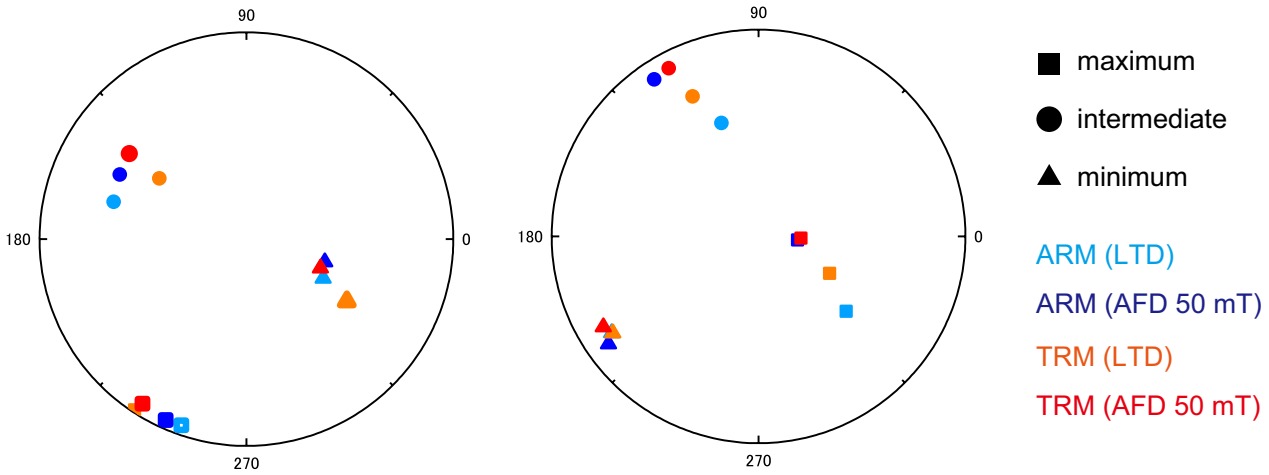

Sample no. 9020

	P_j	T_j
ARM (LTD)	3.23	0.20
ARM (AFD 50 mT)	5.28	0.23
TRM (LTD)	3.65	0.08
TRM (AFD 50 mT)	7.64	0.12

Sample no. 9061

	P_j	T_j
ARM (LTD)	2.98	0.41
ARM (AFD 50 mT)	3.74	0.47
TRM (LTD)	2.76	0.13
TRM (AFD 50 mT)	5.88	0.37

Fig. 12 Representative results on the anisotropy axes measurement on single plagioclase crystals. Sample holder coordinate (not oriented). Left side, sample with prolate anisotropy; right side, sample with oblate anisotropy

along the Y axis seems to be more reproducible for the present sample configuration, though the number of studied samples was not enough to determine which protocol was more suitable.

We found that ARM was larger than TRM in all plagioclase samples, in contrast to the whole-rock sample. This has been reported as a peculiar feature of exsolved magnetite by Usui et al. (2015).

Remanence anisotropy of plagioclase

ARM anisotropy tensors were estimated from the measured ARM_x, ARM_y, and ARM_z for each plagioclase grain. Eigenvalues and anisotropy parameters, corrected anisotropy degree P_j, and shape factor T_j (Jelinek 1981) were calculated (Table 2). Positive and negative values of T_j indicate that the shape of the anisotropy ellipsoids is oblate and prolate, respectively. Median of P_j is 3.35 and T_j varies from $+0.72$ to -0.80. Typical results of analysis on anisotropy directions and anisotropy parameters are shown in Fig. 12. The directions of the anisotropy axes are identical for ARM and TRM, and do not change by AFD. Hence, we used the ARM anisotropy tensor as a proxy for TRM anisotropy tensor in the discussion in "Anisotropy effect on paleointensity" section. P_j increased after AFD, which could be reasonable considering that grains with high aspect ratio correspond to high coercivity components. The whole-rock ARM was isotropic ($P_j = 1.2$, $T_j = -0.28$).

Discussion

Anisotropy effect on paleointensity

Our paleointensity value could be either larger or smaller than the true value depending on angles between the anisotropy axes and directions of ancient or laboratory fields (Paterson 2013). In our paleointensity experiments, anisotropy bias is mainly caused by the directional difference between the external field that gave the NRM, and the laboratory field that gave the ARM0. Since the whole-rock sample was isotropic, the plagioclase grains should be randomly oriented in the host rock assuming that the ARM of whole rock is mainly carried by plagioclase-hosted magnetite. Therefore, the direction of the external field which gave NRM should be random against the anisotropy axes of each plagioclase grain. We calculated the anisotropy bias between two remanence vectors given by randomly oriented external fields with same intensity using the typical anisotropy tensor with eigenvalues (w_1, w_2, w_3) = (1.56, 0.90, 0.49), assuming that the laboratory field was also randomly oriented against the anisotropy axes. Figure 13 shows the anisotropy bias (ratio of the intensity of two remanence vectors) as a function of the angular difference between two remanence vectors (NRM and ARM0). In the present study, we obtained paleointensity results from nine plagioclase samples; the angular difference between NRM and ARM0 for each sample was below 25°. In this condition, the

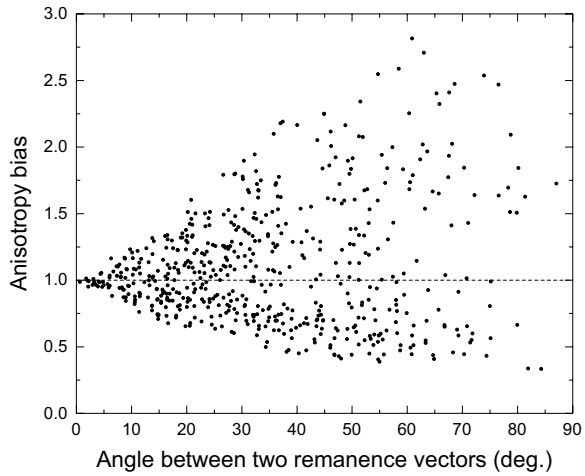

Fig. 13 Anisotropy bias calculated from the typical anisotropy tensor of plagioclase samples as a function of angle between two remanence vectors (here assumed to be NRM and ARM0). An anisotropy bias larger than 1 indicates that the paleointensity is overestimated, and vice versa

anisotropy bias averaged for nine samples was within 1 ± 0.1, and the standard deviation was below 25%. Therefore, anisotropy bias is likely canceled by averaging paleointensity results from nine samples in this study. Also, the variation of the experimental results (~ 20% of the mean value) was consistent with our calculation. We concluded that accurate paleointensity information can be derived from the mean paleointensity values of an assembly of single plagioclase crystals, while the large dispersion of paleointensity values is constitutional for the randomly oriented anisotropic grain assemblage.

Based on anisotropy measurements of plagioclase crystals separated from an Archean granitoid, Usui et al. (2015) demonstrated that (1) geometric mean instead of arithmetic mean should be used, and (2) tens of crystals would be needed to achieve reliable paleointensity estimates. In the present study, the geometric mean and the arithmetic mean are similar in the range of standard deviation, so fewer crystals are required. This difference can be attributed to the variation of the anisotropy effect; the anisotropy tensor they used for estimates was more anisotropic (corresponding to $P_j = 6.21$ and $T_j = 0.34$) than that used in the present study (corresponding to $P_j = 3.18$ and $T_j = 0.04$). Since the shape and fabric of exsolved magnetite vary among samples, the anisotropy effect and how to get rid of it need to be studied carefully for each rock.

In addition to remanence anisotropy, nonlinear TRM acquisition is a major issue of exsolved magnetite paleomagnetism. In the case of the studied sample, the NRM/IRM ratio was lower than the TRM/IRM ratio of previously studied plagioclase crystals (Usui et al. 2015) and rocks containing exsolved magnetite (Selkin et al. 2007). This implies that the nonlinear TRM acquisition may be insignificant for the obtained paleointensity range (~ 60 μT). Also, there is a possibility that NRM of exsolved magnetite is a thermochemical remanent magnetization (TCRM) rather than a TRM since the formation temperature of exsolved magnetite in plagioclase is not clear (Feinberg et al. 2005). In that case, obtained paleointensity could give the lower limit of the field strength at the age, as TCRM acquisition is less efficient than TRM acquisition (Stacey and Banerjee 1974; Usui and Nakamura 2009).

Comparison of magnetic carriers of plagioclase and whole-rock samples

Wakabayashi et al. (2006) and Tsunakawa et al. (2009) predicted that most of the stable remanence of the Iritono granite was carried by magnetite inclusions in plagioclase. However, detailed rock-magnetic experiments on plagioclase grains compared to the previously reported whole-rock studies revealed that the distribution of blocking temperatures and grain sizes are different between plagioclase crystals and the whole rock. The pTRM distributions do not show any concentration in a particular temperature interval below 550 °C for plagioclase samples, while about 10% of the whole-rock TRM is carried by a low blocking temperature (300–500 °C) component. Because the Iritono granite contains magnetite and pyrrhotite ("Rock-magnetic properties of zircon, Rock-magnetic properties of quartz, Rock-magnetic properties of plagioclase" sections; Wakabayashi et al. 2006; Tsunakawa et al. 2009), the low blocking temperature component above 350 °C found in the whole-rock TRM can be attributed to coarse-grained PSD and MD magnetites. Hysteresis loop measurements also indicate that magnetite in plagioclase has a narrow range of grain size compared to the whole rock (Fig. 6d). In addition, the results of the whole-rock experiments exhibit a bimodal distribution according to different paleointensity methods which suggest the influence of non-ideal magnetic minerals, and alternation of such minerals which could not be detected or suppressed completely. On the other hand, plagioclase samples mostly contain nearly-pure, fine-grained magnetite as the magnetic carriers.

Nevertheless, the magnetic carrier of plagioclase crystals and the whole rock was different in terms of distribution of grain size and blocking temperatures, and the estimated paleointensity was consistent among them. Therefore, we conclude that a reliable paleointensity was obtained successfully. Because of the more 'ideal' magnetic carrier, paleointensity experiments on

single plagioclase with exsolved magnetite inclusions can potentially give more reliable and informative paleointensity results than the conventional whole-rock experiments.

Effect of cooling rate on paleointensity

The extremely slow cooling of granitic rocks compared to laboratory timescales may require a correction to the paleointensity estimate due to the time dependence of the acquisition of TRM, which varies by size and aspect ratio of the magnetic grains (Halgedahl et al. 1980; Selkin et al. 2000; Yu 2011). Results on magnetic hysteresis measurements of plagioclase grains are plotted in the PSD region on the Day plot (Fig. 6d), which could be interpreted as a mixture of a range of grain size and aspect ratio. The stable remanence that is involved in paleointensity measurements is carried by SD to PSD magnetite. Based on SD theory (Halgedahl et al. 1980; Selkin et al. 2000) and the estimated cooling time of the Iritono granite body, Tsunakawa et al. (2009) argued that the ratio of TRM in nature to TRM in laboratory would be 1.5 for the SD components. On the other hand, PSD grains have insignificant cooling rate dependence on TRM acquisition (Yu 2011). The cooling rate corrected paleointensity value of 38.2 ± 7.9 μT assuming SD magnetite gives the lower limit of the paleointensity, since the PSD magnetite should give higher paleointensity value. Therefore, corresponding cooling rate corrected VDM value of $8.9 \pm 1.8 \times 10^{22}$ Am^2 using the paleointensity value of plagioclase crystals and inclination of the H component of the whole rock in Wakabayashi et al. (2006) can impose a constraint on the lower limit of paleointensity at the age of 115 Ma.

Significance of Shaw-type paleointensity methods on single crystals

This is the first report applying the Tsunakawa–Shaw paleointensity method to single grain samples. Considering that several results were rejected because of severe alternation during laboratory heating, a Shaw-type method, in which number of heating in laboratory are minimized, seems to be more appropriate than a Thellier-type method. Furthermore, the ThD curves of plagioclase crystals (Fig. 6f) show a very narrow distribution of blocking temperature below the Curie temperature of magnetite (530–580 °C), while the AFD curve (Top-right diagram in Fig. 8) show broad distribution of coercivity (50–150 mT). This emphasizes an advantage to estimate a paleointensity not in a blocking temperature space (by a Thellier-type method) but in a coercivity space (by a Shaw-type method), especially for a magnetically weak sample such as single crystals. Thus the Tsunakawa–Shaw method could be more suitable than the Thellier–Thellier methods in the case of plagioclase sample containing exsolved magnetite, while these methods should be compared in the future paleointensity study using appropriate samples.

Paleointensity during middle CNS

Considering the possible TCRM origin of NRM and the contribution of PSD grains on the cooling rate correction, the VDM value of $8.9 \pm 1.8 \times 10^{22}$ Am^2 gives the lower limit of the time-averaged field strength during the middle age of CNS. Average field strength of the periods of frequent reversals have been estimated as the VDM value of the past 5 million years from the Society Islands volcanic rocks (3.6×10^{22} Am^2; Yamamoto and Tsunakawa 2005), and the virtual axial dipole moment (VADM) value of 0–160 Ma excluding CNS period from submarine basalt glass samples (4.8×10^{22} Am^2; Tauxe 2006). The present result suggests that the time-averaged field strength during middle CNS was several times as large as that of non-superchron periods, supporting the prediction by dynamo models and simulations (e.g. Larson and Olson 1991; Glatzmaier et al. 1999; Kutzner and Christensen 2002; Christensen and Aubert 2006; Olson and Christensen 2006; Courtillot and Olson 2007; Takahashi et al. 2008; Olson et al. 2010). By applying the present paleointensity method to various granitic rocks from different ages, we may be able to improve our understanding of the long-term behavior of the geomagnetic field concerning the mantle convection process without the complications of unideal magnetic minerals that often compromise such work.

Conclusion

We have evaluated the utility of using single silicate crystals separated from granitic rocks in the exploration the long-term evolution of the intensity of the geomagnetic field. We studied the rock-magnetic properties of zircon, quartz and plagioclase separated from the Iritono granite whose paleointensity was already well constrained by past studies using whole-rock samples. In our samples we found that plagioclase was the most suitable mineral phase to study, which was more reliably and stably magnetic than other minerals like zircon or quartz. We conducted paleointensity experiments on 17 plagioclase grains using the Tsunakawa–Shaw method. Nine samples were successful and gave mean paleointensity values of 57.4 ± 11.8 μT. This value is consistent with the previously reported whole-rock paleointensity, suggesting that an assembly of single plagioclase crystals separated from a granitic rock has the ability to yield the accurate

paleointensity data. Considering the unknown forming temperature of exsolved magnetite and cooling rate effect on TRM acquisition, time-averaged VDM is estimated to be higher than $8.9 \pm 1.8 \times 10^{22}$ Am^2 at the age of 115 Ma, suggesting high dipole strength during the middle age of CNS.

Authors' contributions

YY and HT collected the samples. CK conducted the magnetic measurements. All contributed to discussion and writing the manuscript. All authors read and approved the final manuscript.

Author details

[1] Department of Environmental Changes, Faculty of Social and Cultural Studies, Kyushu University, Fukuoka, Japan. [2] Department of Earth and Planetary Sciences, Tokyo Institute of Technology, Tokyo, Japan. [3] Department of Earth and Planetary Science, University of Tokyo, Tokyo, Japan. [4] Center for Advanced Marine Core Research, Kochi University, Kochi, Japan. [5] Division of Geological and Planetary Sciences, California Institute of Technology, Pasadena, USA. [6] Earth-Life Science Institute, Tokyo Institute of Technology, Tokyo, Japan.

Acknowledgements

We thank Shinji Yamamoto for petrological discussions. The microscopic photograph of plagioclase sample (Fig. 7) was taken by Yujiro Tamura. We thank lead guest editor John Tarduno and two anonymous reviewers for their constructive comments. Rock- and paleomagnetic measurements were taken under the cooperative research program of Center for Advanced Marine Core Research (CMCR), Kochi University (Accept Nos. 16A009, 16B009, 17A028 and 17B028). This work was supported by the Japan Society for the Promotion of Science (JSPS) Research Fellowship for Young Scientists (DC1) No. 15J11812.

Competing interests

The authors declare that they have no competing interests.

Availability of data and materials

The data and materials used in this study are available on request to the corresponding author, Chie Kato (chiekato15@gmail.com).

Ethics approval and consent to participate

Not applicable.

Funding

This work was supported by the Japan Society for the Promotion of Science (JSPS) Research Fellowship for Young Scientists (DC1) No. 15J11812.

Publisher's Note

Received: 3 July 2018 Accepted: 25 October 2018
Published online: 13 November 2018

References

Biggin AJ, Strik GH, Langereis CG (2009) The intensity of the geomagnetic field in the late-Archaean: new measurements and an analysis of the updated IAGA palaeointensity database. Earth Planets Space 61(1):9–22. https://doi.org/10.1186/BF03352881

Biggin AJ, Steinberger B, Aubert J, Suttie N, Holme R, Torsvik TH, van der Merr DG, Van Hinsbergen DJJ (2012) Possible links between long-term geomagnetic variations and whole-mantle convection processes. Nat Geosci 5(8):526–533. https://doi.org/10.1038/ngeo1521

Carter-Stiglitz B, Moskowitz B, Jackson M (2001) Unmixing magnetic assemblages and the magnetic behavior of bimodal mixtures. J Geophys Res Solid Earth 106(B11):26397–26411. https://doi.org/10.1029/2001JB000417

Carter-Stiglitz B, Jackson M, Moskowitz B (2002) Low-temperature remanence in stable single domain magnetite. Geophys Res Lett 29(7):33-1. https://doi.org/10.1029/2001GL014197

Channell JET, McCabe C (1994) Comparison of magnetic hysteresis parameters of unremagnetized and remagnetized limestones. J Geophys Res Solid Earth 99(B3):4613–4623. https://doi.org/10.1029/93JB02578

Christensen UR, Aubert J (2006) Scaling properties of convection driven dynamos in rotating spherical shells and application to planetary magnetic fields. Geophys J Int 166:97–114. https://doi.org/10.1111/j.1365-246X.2006.03009.x

Coe RS (1967) Determination of paleo-intensities of the Earth's magnetic field with emphasis on mechanisms which could cause non-ideal behaviour in Thellier's method. J Geomagn Geoelectr 19:157–179

Cottrell RD, Tarduno JA (1999) Geomagnetic paleointensity derived from single plagioclase crystals. Earth Planet Sci Lett 169(1):1–5. https://doi.org/10.1016/S0012-821X(99)00068-0

Cottrell RD, Tarduno JA, Roberts J (2008) The Kiaman Reversed Polarity Superchron at Kiama: toward a field strength estimate based on single silicate crystals. Phys Earth Planet Inter 169(1):49–58. https://doi.org/10.1016/j.pepi.2008.07.041

Courtillot V, Olson P (2007) Mantle plumes link magnetic superchrons to Phanerozoic mass depletion events. Earth Planet Sci Lett 260(3):495–504. https://doi.org/10.1016/j.epsl.2007.06.003

Day R, Fuller M, Schmidt VA (1977) Hysteresis properties of titanomagnetites: grain-size and compositional dependence. Phys Earth Planet Int 13(4):260–267. https://doi.org/10.1016/0031-9201(77)90108-X

Dunlop DJ, Özdemir Ö (1997) Rock magnetism—fundamentals and frontiers. Cambridge University Press, Cambridge

Feinberg JM, Scott GR, Renne PR, Wenk HR (2005) Exsolved magnetite inclusions in silicates: features determining their remanence behavior. Geology 33(6):513–516. https://doi.org/10.1130/G21290.1

Fu RR, Weiss BP, Lima EA, Kehayias P, Araujo JFDF, Glenn DR, Gelb J, Einsle JF, Bauer AM, Harrison RJ, Ali GAH, Walsworth RL (2017) Evaluating the paleomagnetic potential of single zircon crystals using the Bishop Tuff. Earth Planet Sci Lett 458:1–13. https://doi.org/10.1016/j.epsl.2016.09.038

Glatzmaier GA, Coe RS, Hongre L, Roberts PH (1999) The role of the Earth's mantle in controlling the frequency of geomagnetic reversals. Nature 401(6756):885–890. https://doi.org/10.1038/44776

Halgedahl SL, Day R, Fuller M (1980) The effect of cooling rate on the intensity of weak-field TRM in single-domain magnetite. J Geophys Res Solid Earth 85(B7):3690–3698. https://doi.org/10.1029/JB085iB07p03690

Heider F, Dunlop DJ, Soffel HC (1992) Low-temperature and alternating field demagnetization of saturation remanence and thermoremanence in magnetite grains (0.037 μm to 5 mm). J Geophys Res Solid Earth 97(B6):9371–9381. https://doi.org/10.1029/91jb03097

Jelinek V (1981) Characterization of the magnetic fabric of rocks. Tectonophysics 79(3–4):T63–T67. https://doi.org/10.1016/0040-1951(81)90110-4

Kosterov A (2003) Low-temperature magnetization and AC susceptibility of magnetite: effect of thermomagnetic history. Geophys J Int 154(1):58–71. https://doi.org/10.1046/j.1365-246X.2003.01938.x

Kutzner C, Christensen U (2002) From stable dipolar towards reversing numerical dynamos. Phys Earth Planet Int 121:29–45. https://doi.org/10.1016/S0031-9201(02)00016-X

Larson RL, Olson P (1991) Mantle plumes control magnetic reversal frequency. Earth Planet Sci Lett 107(3–4):437–447. https://doi.org/10.1016/0012-821X(91)90091-U

Mochizuki N, Tsunakawa H, Oishi Y, Wakai S, Wakabayashi KI, Yamamoto Y (2004) Palaeointensity study of the Oshima 1986 lava in Japan: implications for the reliability of the Thellier and LTD-DHT Shaw methods. Phys Earth Planet Inter 146(3):395–416. https://doi.org/10.1016/j.pepi.2004.02.007

Moskowitz BM, Frankel RB, Bazylinski DA (1993) Rock magnetic criteria for the detection of biogenic magnetite. Earth Planet Sci Lett 120(3–4):283–300. https://doi.org/10.1016/0012-821X(93)90245-5

Moskowitz BM, Jackson M, Kissel C (1998) Low-temperature magnetic behavior of titanomagnetites. Earth Planet Sci Lett 157:141–149. https://doi.org/10.1016/S0012-821X(98)00033-8

Muxworthy AR, Evans ME (2012) Micromagnetics and magnetomineralogy of ultrafine magnetite inclusions in the Modipe Gabbro. Geochem Geophys Geosyst 14(4):921–928. https://doi.org/10.1029/2012GC004445

Olson P, Christensen UR (2006) Dipole moment scaling for convection-driven planetary dynamos. Earth Planet Sci Lett 250:561–571. https://doi.org/10.1016/j.epsl.2006.08.008

Olson PL, Coe RS, Driscoll PE, Glatzmaier GA, Roberts PH (2010) Geodynamo reversal frequency and heterogeneous core–mantle boundary heat flow. Phys Earth Planet Int 180(1–2):66–79. https://doi.org/10.1016/j.pepi.2010.02.010

Özdemir Ö, Dunlop DJ, Moskowitz BM (1993) The effect of oxidation on the Verwey transition in magnetite. Geophys Res Lett 20(16):1671–1674. https://doi.org/10.1029/93GL01483

Parry LG (1982) Magnetization of immobilized particle dispersions with two distinct particle sizes. Phys Earth Planet Int 28(3):230–241. https://doi.org/10.1016/0031-9201(82)90004-8

Paterson GA (2013) The effects of anisotropic and non-linear thermoremanent magnetizations on Thellier-type paleointensity data. Geophys J Int 193(2):694–710. https://doi.org/10.1093/gji/ggt033

Sato M, Yamamoto S, Yamamoto Y, Okada Y, Ohno M, Tsunakawa H, Maruyama S (2015) Rock-magnetic properties of single zircon crystals sampled from the Tanzawa tonalitic pluton, central Japan. Earth Planets Space 67(1):150. https://doi.org/10.1186/s40623-015-0317-9

Selkin PA, Gee JS, Tauxe L, Meurer WP, Newell AJ (2000) The effect of remanence anisotropy on paleointensity estimates: a case study from the Archean Stillwater Complex. Earth Planet Sci Lett 183(3):403–416. https://doi.org/10.1016/S0012-821X(00)00292-2

Selkin PA, Gee JS, Tauxe L (2007) Nonlinear thermoremanence acquisition and implications for paleointensity data. Earth Planet Sci Lett 256(1):81–89. https://doi.org/10.1016/j.epsl.2007.01.017

Selkin PA, Gee JS, Meurer WP, Hemming SR (2008) Paleointensity record from the 2.7 Ga Stillwater Complex, Montana. Geochem Geophys Geosyst. https://doi.org/10.1029/2008gc001950

Shcherbakova VV, Bakhmutov VG, Shcherbakov VP, Zhidkov GV, Shpyra VV (2012) Palaeointensity and palaeomagnetic study of Cretaceous and Palaeocene rocks from Western Antarctica. Geophys J Int 189(1):204–228. https://doi.org/10.1111/j.1365-246X.2012.05357.x

Stacey FD, Banerjee SK (1974) The physical principles of rock magnetism. Elsevier, New York

Takahashi F, Tsunakawa H, Matsushima M, Mochizuki N, Honkura Y (2008) Effects of thermally heterogeneous structure in the lowermost mantle on the geomagnetic field strength. Earth Planet Sci Lett 272(3):738–746. https://doi.org/10.1016/j.epsl.2008.06.017

Tanaka H, Kono M (2002) Paleointensities from a Cretaceous basalt platform in Inner Mongolia, northeastern China. Phys Earth Planet Int 133(1):147–157. https://doi.org/10.1016/S0031-9201(02)00091-2

Tarduno JA, Cottrell RD, Smirnov AV (2001) High geomagnetic intensity during the mid-Cretaceous from Thellier analyses of single plagioclase crystals. Science 291(5509):1779–1783. https://doi.org/10.1126/science.1057519

Tarduno JA, Cottrell RD, Smirnov AV (2002) The Cretaceous superchron geodynamo: observations near the tangent cylinder. Proc Natl Acad Sci 99:14020–14025. https://doi.org/10.1073/pnas.222373499

Tarduno JA, Cottrell RD, Smirnov AV (2006) The paleomagnetism of single silicate crystals: recording geomagnetic field strength during mixed polarity intervals, superchrons, and inner core growth. Rev Geophys. https://doi.org/10.1029/2005rg000189

Tarduno JA, Cottrell RD, Watkeys MK, Bauch D (2007) Geomagnetic field strength 3.2 billion years ago recorded by single silicate crystals. Nature 446(7136):657–660. https://doi.org/10.1038/nature05667

Tarduno JA, Cottrell RD, Watkeys MK, Hofmann A, Doubrovine PV, Mamajek EE, Liu D, Sibeck DG, Neukirch LP, Usui Y (2010) Geodynamo, solar wind, and magnetopause 3.4 to 3.45 billion years ago. Science 327(5970):1238–1240. https://doi.org/10.1126/science.1183445

Tarduno JA, Blackman EG, Mamajek EE (2014) Detecting the oldest geodynamo and attendant shielding from the solar wind: Implications for habitability. Phys Earth Planet Int 233:68–87. https://doi.org/10.1016/j.pepi.2014.05.007

Tarduno JA, Cottrell RD, Davis WJ, Nimmo F, Bono RK (2015) A Hadean to Paleoarchean geodynamo recorded by single zircon crystals. Science 349(6247):521–524. https://doi.org/10.1126/science.aaa9114

Tauxe L (2006) Long-term trends in paleointensity: the contribution of DSDP/ODP submarine basaltic glass collections. Phys Earth Planet Inter 156(3):223–241. https://doi.org/10.1016/j.pepi.2005.03.022

Thellier E, Thellier O (1959) Sur l'intensite du champ magnetique terrestre dans le passe historique et geologique. Ann Geophys 15:285–376

Tsunakawa H, Shaw J (1994) The Shaw method of palaeointensity determinations and its application to recent volcanic rocks. Geophys J Int 118(3):781–787. https://doi.org/10.1111/j.1365-246X.1994.tb03999.x

Tsunakawa H, Wakabayashi KI, Mochizuki N, Yamamoto Y, Ishizaka K, Hirata T, Takahashi F, Seita K (2009) Paleointensity study of the middle Cretaceous Iritono granite in northeast Japan: implication for high field intensity of the Cretaceous normal superchron. Phys Earth Planet Int 176(3):235–242. https://doi.org/10.1016/j.pepi.2009.07.001

Usui Y (2013) Paleointensity estimates from oceanic gabbros: effects of hydrothermal alteration and cooling rate. Earth Planets Space 65(9):985–996. https://doi.org/10.5047/eps.2013.03.015

Usui Y, Nakamura N (2009) Nonlinear thermoremanence corrections for Thellier paleointensity experiments on single plagioclase crystals with exsolved magnetites: a case study for the Cretaceous Normal Superchron. Earth Planets Space 61(12):1327–1337. https://doi.org/10.1186/BF03352985

Usui Y, Shibuya T, Sawaki Y, Komiya T (2015) Rock magnetism of tiny exsolved magnetite in plagioclase from a Paleoarchean granitoid in the Pilbara craton. Geochem Geophys Geosyst 16(1):112–125. https://doi.org/10.1002/2014GC005508

Wakabayashi KI, Tsunakawa H, Mochizuki N, Yamamoto Y, Takigami Y (2006) Paleomagnetism of the middle Cretaceous Iritono granite in the Abukuma region, northeast Japan. Tectonophysics 421(1):161–171. https://doi.org/10.1016/j.tecto.2006.04.013

Weiss BP, Maloof AC, Tailby N, Ramezani J, Fu RR, Hanus V, Trail D, Watson EB, Harrison TM, Bowring SA, Kirschvink JL, Swanson-Hysell NL, Coe RS (2015) Pervasive remagnetization of detrital zircon host rocks in the Jack Hills, Western Australia and implications for records of the early geodynamo. Earth Planet Sci Lett 430:115–128. https://doi.org/10.1016/j.epsl.2015.07.067

Wenk HR, Chen K, Smith R (2011) Morphology and microstructure of magnetite and ilmenite inclusions in plagioclase from Adirondack anorthositic gneiss. Am Min 96(8–9):1316–1324. https://doi.org/10.2138/am.2011.3760

Tarduno JA, Cottrell RD (2005) Dipole strength and variation of the time-averaged reversing and nonreversing geodynamo based on Thellier analyses of single plagioclase crystals. J Geophys Res Solid Earth. https://doi.org/10.1029/2005jb003970

Yamamoto Y, Tsunakawa H (2005) Geomagnetic field intensity during the last 5 Myr: ITD-DHT Shaw palaeointensities from volcanic rocks of the Society Islands, French Polynesia. Geophys J Int 162(1):79–114. https://doi.org/10.1111/j.1365-246X.2005.02651.x

Yamamoto Y, Tsunakawa H, Shibuya H (2003) Palaeointensity study of the Hawaiian 1960 lava: implications for possible causes of erroneously high intensities. Geophys J Int 153(1):263–276. https://doi.org/10.1046/j.1365-246X.2003.01909.x

Yamamoto Y, Torii M, Natsuhara N (2015) Archeointensity study on baked clay samples taken from the reconstructed ancient kiln: implication for validity of the Tsunakawa–Shaw paleointensity method. Earth Planets Space 67(1):63. https://doi.org/10.1186/s40623-015-0229-8

Yu Y (2010) Paleointensity determination using anhysteretic remanence and saturation isothermal remanence. Geochem Geophys Geosyst. https://doi.org/10.1029/2009gc002804

Yu Y (2011) Importance of cooling rate dependence of thermoremanence in paleointensity determination. J Geophys Res Solid Earth. https://doi.org/10.1029/2011jb008388

Yu Y, Tauxe L, Genevey A (2004) Toward an optimal geomagnetic field intensity determination technique. Geochem Geophys Geosyst. https://doi.org/10.1029/2003gc000630

Zhang N, Zhong S (2011) Heat fluxes at the Earth's surface and core–mantle boundary since Pangea formation and their implications for the geomagnetic superchrons. Earth Planet Sci Lett 306(3–4):205–216. https://doi.org/10.1016/j.epsl.2011.04.001